Single photon detection at visible and x-ray wavelengths with Nb–Al superconducting tunnel junctions

P. Verhoeve,[a] N. Rando, A. Peacock, A. van Dordrecht, and A. Poelaert
Astrophysics Division, Space Science Department of the European Space Agency, Estec, P.O. Box 299, 2200 AG Noordwijk, The Netherlands

D. J. Goldie
Oxford Instruments Scientific Research Division, Newton House, Cambridge Business Park, Cowley Road, Cambridge CB4 4WZ, England

R. Venn
Cambridge Microfab Ltd, Trollheim Cranes Lane, Kingston, Cambridge CB3 7NJ, England

(Received 12 December 1997; accepted for publication 11 February 1998)

Photon counting experiments at wavelengths ranging from near infrared to x-ray with niobium based superconducting tunnel junctions with aluminum trapping layers are presented. Single photons can be detected up to a wavelength of 1 μm. The response in the ultraviolet to near-infrared region is characterized by a good energy linearity ($<2.5\%$), a capability to handle event rates up to ~ 3 kHz, and moderate energy resolving power ($E/\Delta E \approx 7$ for $E=4$ eV). The x-ray response at 6 keV is characterized by anomalously high signals compared to the low energy response, a severe energy nonlinearity and a relatively poor energy resolution of ~ 140 eV, full width at half maximum. © *1998 American Institute of Physics.* [S0021-8979(98)04010-9]

I. INTRODUCTION

Superconducting tunnel junctions (STJs) have been extensively studied in the last decade in pursuit of the predicted excellent energy resolving power at x-ray photon energies.[1] The high energy resolution, compared to semiconductor- or gas-based detectors, arises from the much lower energy necessary to generate free-charge carriers. In the case of a superconductor, these free charge carriers (quasiparticles) are produced by the breaking of Cooper pairs, which typically requires an energy of the order of $\sim$ meV. For a widely used superconducting material such as Nb, it has been calculated that the number of quasiparticles produced by the absorption of a photon with energy E is given as

$$N_0(E)=\frac{E}{\epsilon}\pm\sqrt{\frac{F}{\epsilon}F}. \tag{1}$$

Here $\epsilon\sim 1.7\Delta$ (with Δ the band gap of the superconductor) is the average energy required to generate one quasiparticle and $F=0.22$ is the Fano factor.[2,3] The quasiparticles can be detected through tunneling, by means of a number of different tunnel processes across the thin insulating barrier of a STJ. The amplitude of the signal pulse measured after the absorption of a photon will, in a first approximation, be proportional to the number of generated quasiparticles and, thus, to the energy of the photon. If each quasiparticle would induce exactly one tunnel process, the limiting energy resolution [full width at half maximum (FWHM)] for a 6 keV x-ray photon would be ~ 4 eV. In most practical applications, however, the probabilities P_1 and P_2 for a tunnel process from the electrode where the photon absorption took place (1) to the opposite electrode (2), and vice versa, will be less than unity. These probabilities are dependent on the rates for tunneling across the barrier (Γ_{tun}) and the rates for loss of quasiparticles from the electrode (Γ_{loss}) by mechanisms other than by tunneling, such as recombination, trapping in lower band gap regions or diffusion into the connecting leads. The probability for tunneling from electrode i can be written as

$$P_i=\frac{\Gamma_{\text{tun},i}}{\Gamma_{\text{tun},i}+\Gamma_{\text{loss},i}}. \tag{2}$$

Thus, the number of detected quasiparticles $N(E)$ will be,[4]

$$N(E)=\langle n\rangle\left[N_0(E)\pm\sqrt{\frac{E}{\epsilon}(F+G)}\right] \tag{3a}$$

with $\langle n\rangle$ the average number of tunnel processes per quasiparticle given by

$$\langle n\rangle=\frac{P_1(1+P_2)}{(1-P_1P_2)} \tag{3b}$$

and the tunnel noise factor G given by

$$G=\frac{P_1-P_1^2+3P_1P_2+P_1^2P_2}{(P_1+P_1P_2)^2}. \tag{3c}$$

Typically, the energy resolution of a niobium based STJ will be dependent on statistical fluctuations in $N_0(E)$ and n, and be of order $\sim 10-15$ eV for 6 keV x rays. Further degradation of the energy resolution can be envisaged due to spatial nonuniformities in the response of the detector and to electronic noise. For a symmetrical device[5,4] ($P_i=P_j$), $G=1+1/\langle n\rangle$ and the measured energy resolution can be approximated by

[a]Electronic mail: pverhoev@astro.estec.esa.nl

$$\Delta E = 2.355\sqrt{\epsilon E(F+1+G)+(\alpha E)^2+(\sigma_{\text{electr.}})^2}, \qquad (4)$$

where α is a device dependent constant (in eV per eV of photon energy) quantifying the resolution degradation due spatial nonuniformity in the response,[6] and σ_{electr} is the electronic noise contribution. While several groups have achieved energy resolutions better than 100 eV FWHM at 5.89 keV, the best results reported to date are 29 eV by Mears *et al.*,[7] for a Nb-based device with 200 nm thick Al trapping layers, and 27 eV by Hettl *et al.*,[8] for an Al device.

A second attractive prospect of superconducting detectors lies in their application as photon counting detectors with a moderate intrinsic energy resolving power for ultraviolet (uv) and visible light. These properties, in combination with a relatively high detection efficiency, make the STJ an important new type of detector for uv/optical applications in astronomy.[9–12] At a typical photon energy of 3 eV ($\lambda \approx 410$ nm), the expected tunnel noise limited energy resolution of a niobium based device will be ~ 0.3 eV (FWHM). The use of materials with lower band gap would have even better prospects, albeit at the cost of a lower operating temperature.[11,12] Spatial nonuniformities in the detector's response will be relatively less important, since their contributions to the energy resolution are proportional to the photon energy. For example, spatial nonuniformities giving rise to $\Delta E \approx 100$ eV at $E = 6$ keV, would have a completely negligible effect on the energy resolution at $E = 3$ eV. The crucial parameter for the detection of low energy photons is the signal-to-noise ratio. The signal can be enhanced by a low resistivity tunnel barrier and by the application of quasiparticle trapping layers,[13] which confine the quasiparticles close to the tunnel barrier. This will enhance the tunnel probability and keep the quasiparticles away from some potential loss sites, such as the oxide coated top surface. Low noise operation requires a high quality tunnel barrier with low leakage current density. Since both the signal as well as the electronic noise depend on the dimensions of the device, these can be optimised for maximum signal-to-noise ratio. Note the signal depends in part on the electrode volume due to quasiparticle loss at the edges and quasiparticle self-recombination, while the noise is a function of device capacitance and subgap current, which depend on the barrier area.

In this work we describe photon counting experiments with niobium-based STJs with Al trapping layers which are optimized for low energy photon detection. Preliminary data on the x-ray performance[14] and on the uv/optical performance[10,15,16] of these devices have been reported in previous papers. In the present article new measurements on the single photon counting capabilities of the same detectors in the uv to near infrared (NIR) wavelength range are presented and a comparison with the detectors response at x-ray wavelengths is made.

II. DESCRIPTION OF THE STJs

The STJs used for this work have been fabricated by Oxford Instruments Scientific Research Division (Cambridge, UK). The detector chip carries eight STJs: four $20\times20\ \mu\text{m}^2$ and four $50\times50\ \mu\text{m}^2$ sized devices. They are

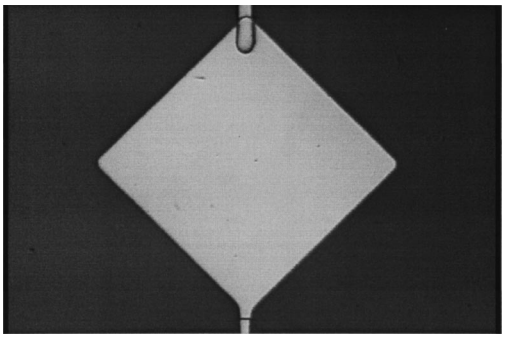

FIG. 1. Nomarski microscope photograph of a $50\times50\ \mu\text{m}^2$ STJ.

Nb–Al–aluminum oxide–Al–Nb multilayers deposited on polished sapphire substrates. Figure 1 shows a Nomarski microscope image of one of the $50\times50\ \mu\text{m}^2$ devices on the chip. The width of the leads is 3 μm. The base and top electrodes of the devices have identical layer thicknesses: 100 nm of niobium and 120 nm of aluminum. The base film niobium is epitaxial, with a residual resistance ratio of ~ 70, whereas the top electrode is polycrystalline. The aluminum oxide barrier has an estimated thickness of <1 nm and a resistance of $\sim 2.2\times10^{-6}\ \Omega\ \text{cm}^2$. The band gap of the devices at the barrier, as derived from the current–voltage ($I-V$) curves and assuming equal gaps in top and base electrode, is 0.44 mV. In spite of the very high electron transmissivity, the junctions show low leakage currents. This is illustrated in Figs. 2(a) and 2(b), which show the $I-V$ characteristic at $T = 0.3$ K and the measured subgap current densities in the temperature range 0.3–1.1 K for a $20\times20\ \mu\text{m}^2$ device, respectively. The solid line in Fig. 2(b) is the calculated subgap current density for a Bardeen–Cooper–Schrieffer (BCS)-like temperature dependence using the above mentioned band gap and barrier resistance. The measured current density at $T = 0.3$ K could vary between different cooling cycles, indicative of different degrees of trapping of magnetic flux. From the lowest measured current density (which was similar for the best 20×20 and $50\times50\ \mu\text{m}^2$ micron devices) it is concluded that the real leakage current density (as opposed to excess current induced by trapped flux) can only be established at $T<0.3$ K. This leakage current density is of the same order of magnitude ($\leqslant 0.1\ \text{pA}/\mu\text{m}^2$) as in similar niobium-based devices with thin (5 nm) Al layers. For the purpose of single photon counting in the visible wavelength range, where the signals from the STJ are small, a low subgap current at the bias point is essential for low noise performance. The measured subgap current I_{sg} and dynamical resistance R_d of the $20\times20\ \mu\text{m}^2$ device at a typical bias voltage $V_{\text{bias}} = 0.20$ mV and under the most favorable conditions ($T = 0.3$ K and minimal flux trapping problems) were $I_{\text{sg}} = 100$ pA and $R_d \approx 1\ \text{M}\Omega$. Any deviation from these conditions resulted in increased noise.

The characteristic times for trapping of quasiparticles from Nb into the trap formed by the proximised Nb and the Al, as well as the characteristic times for excitation from the trap and for tunneling from the trap across the barrier have been estimated previously,[14] using the work of Golubov *et al.*[17] on the proximity effect in dirty superconductors. It

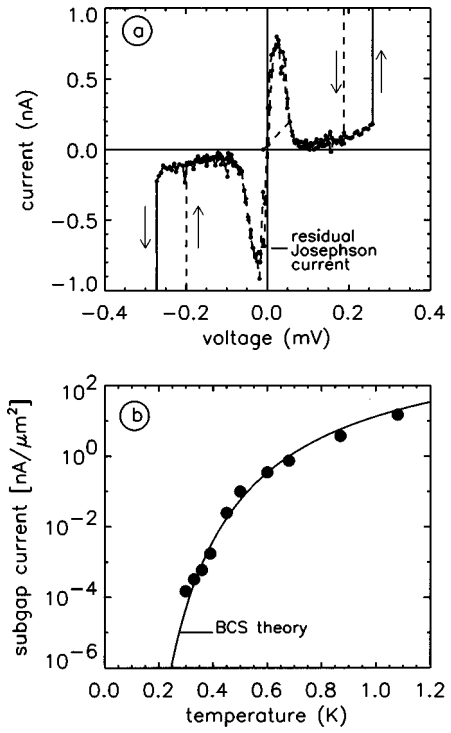

FIG. 2. (a) Part of the $I-V$ characteristic for the $20\times20\ \mu m^2$ device at $T=300$ mK and $B=8$ mT. The structure around zero voltage is the incompletely suppressed Josephson current. The arrows indicate the scanning direction. (b) Measured subgap current density (at $V_{bias}=0.10$ mV) against temperature for the $20\times20\ \mu m^2$ device. The solid line is the calculated current density without leakage current.

was found that the trapping time $\tau_{tr}<1$ ns, whereas the excitation time is on the microsecond time scale. Furthermore, in experiments on similar devices[6] with thin Al layers a typical quasiparticle loss time of the order 1 μs is derived. Therefore, as an approximation it is assumed that all quasiparticles initially created by photon absorption in the Nb layers are instantaneously collected in the trapping regions. Subsequently, tunnel and loss processes begin. The tunnel time, calculated from the approximation given by de Korte *et al.*[18] and taking into account that the trapping layer extends significantly into the Nb,[19] is estimated as $\tau_{tun}\approx0.31\ \mu$s from

$$\tau_{tun}=4e^2R_nA[N_{Al}(0)d_{Al}+N_{Nb}(0)d_{Nb}^{trap}]\times\sqrt{\frac{(\Delta+V_{bias})^2-\Delta^2}{(\Delta+V_{bias})^2}}. \quad (5)$$

Here, R_n is the normal resistance, A is the area of the junction, $N_{Nb}(0)$ and $N_{Al}(0)$ are the normal state single spin densities of state of Nb and Al, d_{Nb}^{trap} and d_{Al} are the effective confinement lengths in the proximised Nb (~12 nm) and the thickness of the Al layer, respectively, and V_{bias} is the applied bias voltage (typically 0.2 mV). A lower limit for $\tau_{tun}\approx0.21\ \mu$s is found if only the Al thickness is taken as the confinement length. Note that the proximity model used here does not strictly apply in case of the clean epitaxial base film Nb and the relatively thick Al layers.

During their relaxation from the gap energy in the bulk Nb ($\Delta_{Nb}^{bulk}\approx1.5$ meV) to the gap energy in the trapping region ($\Delta_{Al}^{trap}=0.44$ meV) the quasiparticles will emit phonons of (just) sufficient energy ($E_{relaxation}\approx1$ meV) to break one additional Cooper pair in the trap. Taking into account phonon losses from the trap, an effective quasiparticle multiplication factor of ~2 has been estimated.[14] Thus, the aluminum trapping layers have a threefold effect on the responsivity of the detectors. First, the quasiparticles are confined in a narrow region close to the barrier, which enhances the tunnel rate. Second, the quasiparticles are kept away from the top electrodes top surface, which has been found to act as a quasiparticle sink.[20] Third, in the process of relaxation to the gap energy in the trap, the original number of quasiparticles is amplified by a factor of ~2.

III. EXPERIMENTAL CONFIGURATION

All experiments in the present work have been performed in a ^{3}He cryostat with a base temperature of ~300 mK. A superconducting magnet provides the magnetic field required to suppress the STJ's Josephson current and Fiske steps. The typical field strength used in the present experiments was of the order of 8 mT.

The light source in the uv and optical experiments was a xenon lamp in combination with a grating monochromator with adjustable entrance slit. An additional filter was used if suppression of light in higher orders of the monochromator was required. A uv-grade silica fiber was used to couple the light into the inner vacuum chamber of the cryostat and onto the detector. The available wavelength range is 200–1060 nm (corresponding to the energy range 1.17–6.2 eV) and is limited at the short wavelength side by the transmission of the fiber and at the long wavelength side by the rotation of the grating. The end of the fiber was at a distance of 0.5–1 mm from the detectors surface, thus illuminating all STJs on the chip more or less uniformly. For practical reasons, the angle of incidence with respect to the plane of the detector was $\sim30°$. The optical constants of niobium in the available wavelength range[21] guarantee complete absorption of the incident light within the 100 nm thickness of Nb of either the base or the top electrode of the STJs. Furthermore, the sapphire substrate is transparent between 200 and 1000 nm. Thus, the top and base electrode of the STJs can be stimulated selectively by illuminating the front or the back side of the detector chip, respectively. The photon flux incident on a STJ is adjustable with the entrance slit of the monochromator. In order to allow for photon counting the photon flux is generally maintained at below 1000 detected photons/s, so that the mean arrival time between photons is far longer than the event processing time of the electronics or the signal pulse duration. This can only be achieved with the entrance slit of the monochromator almost closed, which has the additional advantage of reducing the input bandwidth to a negligible value in this experiment ($\ll5$ nm). However, at monochromator settings of $\lambda<300$ nm, some broad band false light (with $\lambda>500$ nm) is found in the output of the monochromator.

The source in the x-ray experiments is a radioactive ^{55}Fe sample emitting the Mn K_α ($E=5895$ eV) and K_β ($E=6490$ eV) line complexes. This source illuminates the STJs

uniformly at the front side and its intensity is chosen such that typically a few hundred photons/s are detected. Note that, contrary to the uv/optical experiments, 6 keV x-ray photons are absorbed equally in the top and the base electrode ($\sim 2\%$), as well as in the sapphire substrate beneath the STJ ($\sim 96\%$).

The electronics chain used to read out the STJs consists of a charge sensitive preamplifier at ~ 1 m from the STJ, and a shaping stage, both at room temperature. Different electronics chains are used for the optical and x-ray experiments, tuned (so as to maximize the signal-to-noise ratio) to the different magnitudes of the current pulses from the detector. The limiting noise levels of the electronics with open input correspond to ~ 400 and $\sim 6\times 10^4$ electrons rms, for the optical and x-ray experiments, respectively. Pulses from an electronic pulser can be fed into the electronics. The total electronic noise of the combination of STJ and electronics can be measured as the width of the pulse height distribution from this electronic pulser. The electronics chain is optically coupled to a PC. For each detected photon the charge output, which corresponds to the total number of tunneled electrons $N(E)$ as a result of the absorption of one photon, and the rise time of the charge pulse, which corresponds to the decay time of the current pulse from the STJ, are stored on the PC. The time required to detect and process one event amounts to $\sim 160\ \mu$s, and is governed by the bipolar filtering circuit of the pulse shaping stage. While the photon arrival time can be determined to below 10 μs, the current electronics processing time constrains the maximum photon input rate.

IV. RESULTS

A. Ultraviolet and visible light experiments

1. Responsivity and energy linearity

The uv and visible light experiments have concentrated on the $20\times 20\ \mu\text{m}^2$ device, which proved to give the best results. Only limited data is available for the $50\times 50\ \mu\text{m}^2$ device. Single photon pulse height spectra in the wavelength range $\lambda = 200-1000$ nm were acquired in front as well as back illumination. Examples of spectra in back illumination mode at $\lambda = 250$, 500, and 1000 nm are shown in Fig. 3. The responsivity (in electrons per eV of photon energy) and the total electronic noise have been measured as a function of operating temperature and bias voltage across the STJ, in order to determine the optimum operating conditions. Figures 4(a) and 4(b) show the measured responsivity (in back illumination mode) of the $20\times 20\ \mu\text{m}^2$ device and the $50\times 50\ \mu\text{m}^2$ device, respectively, as a function of bias voltage for different temperatures. Measurements at higher temperatures or higher bias voltages were prohibited by excessive noise. Within the accuracy of the measurements, the responsivity of the top electrode (as measured in front illumination) and the base electrode were found to be the same. The conditions for optimum signal-to-noise ratio for the $20\times 20\ \mu\text{m}^2$ were: $V_{\text{bias}}=0.25$ mV and $T=300-330$ mK. In these conditions, the measured responsivity of the $20\times 20\ \mu\text{m}^2$ device is ~ 3000 electrons/eV and the noise is ~ 700 electrons rms. The optimum conditions for the $50\times 50\ \mu\text{m}^2$ device were $V_{\text{bias}}=0.20$ mV and $T=300$ mK,

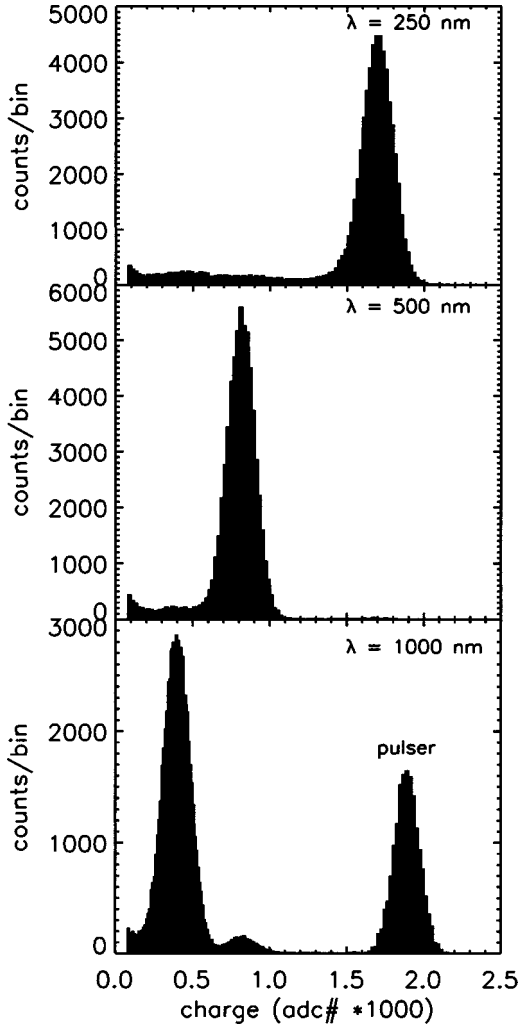

FIG. 3. Pulse height spectra at (a) $\lambda = 250$ nm, (b) $\lambda = 500$ nm, and (c) $\lambda = 1000$ nm from the $20\times 20\ \mu\text{m}^2$ device in back illumination mode. The experimental conditions were: $T=300$ mK, $V_{\text{bias}}=0.25$ mV, and $B=8$ mT. The second peak in the 1000 nm spectrum originates from incomplete suppression of $\lambda = 500$ nm photons from the second order of the monochromator.

yielding a responsivity of ~ 3600 electrons/eV and a noise of ~ 1200 electrons rms. The measured rise times are of the order of 1.5–2 μs for both devices. Assuming that all initial quasiparticles are trapped into the proximised Nb and Al layers and that a quasiparticle multiplication factor of 2 is achieved during the energy relaxation,[14] the average number of tunnel processes per quasiparticle in the trap amounts to ~ 4 for the $20\times 20\ \mu\text{m}^2$ device and ~ 5 for the $50\times 50\ \mu\text{m}^2$ device. If the minimum photon energy detectable in a photon counting experiment is defined as equivalent to $5\sigma_{\text{noise}}$, the maximum detectable wavelengths are $\lambda = 1060$ nm and $\lambda = 740$ nm for the 20×20 and the $50\times 50\ \mu\text{m}^2$ device, respectively.

The strong dependence of the responsivity of the $20\times 20\ \mu\text{m}^2$ device on temperature is remarkable. In the $50\times 50\ \mu\text{m}^2$ device this dependence was less pronounced: $\sim 3\%$ increase in responsivity for $T=300\rightarrow 330$ mK, compared to $\sim 15\%$ for the $20\times 20\ \mu\text{m}^2$ device. This temperature dependence of the responsivity can be interpreted as a

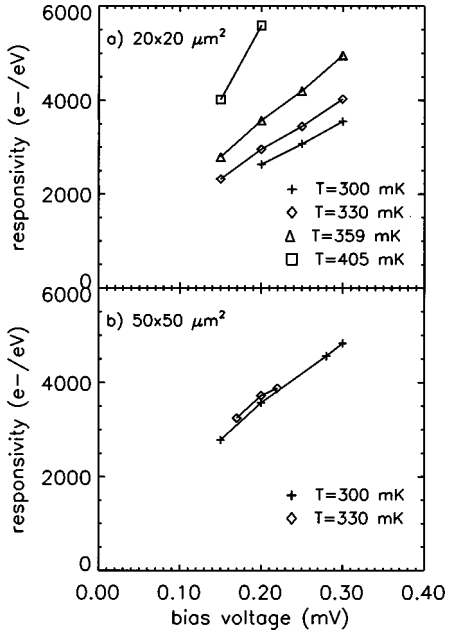

FIG. 4. The responsivity (as measured from single photon pulse height spectra at $\lambda = 470$ nm) as function of bias voltage for: (a) the $20\times 20\ \mu m^2$ and (b) the $50\times 50\ \mu m^2$ at different temperatures. Note how the responsivity increases with increasing device temperature.

temperature dependence of the excess loss rates for quasiparticles. Excess loss processes of quasiparticles are understood to be loss processes through mechanisms other than the unavoidable thermal and self-recombination of quasiparticles, such as trapping and loss in regions of reduced energy gap, for example at the edges of the devices. At elevated temperatures such trapping processes would be counteracted by a higher excitation rate out of the trapping region. This is supported by the smaller temperature effect in the larger device, for which the losses at the edges are a less dominant effect[20] and, hence, also the responsivity is higher.

Figure 5 shows the measured peak positions (obtained from least squares fits to a Gaussian) as a function of photon energy ($E = 6.2-1.4$ eV, $\lambda = 200-900$ nm) for the $20\times 20\ \mu m^2$ device in back-illumination mode. During the measurements, three reference measurements at $\lambda = 300$ nm were taken, from which a drift in the measured charge Q of 1.3% over the complete set is derived. The data in Fig. 5 have been corrected for this drift. A least squares fit of the data to a linear relation between charge and energy yielded an electronic offset of -430 electrons and a responsivity of 2980 electrons/eV. This fit is represented by the solid line in Fig. 5. The deviations from linearity are within 2.5%, indicating a good energy linearity of the detector in this wavelength range.

2. Energy resolution

The energy resolution of the detector has been determined by fitting Gaussians to the single photon peaks in the spectra. The obtained FWHM energy resolutions (in eV) are plotted as a function of photon energy in Figs. 6(a) and 6(b) for back and front illumination modes of the $20\times 20\ \mu m^2$ device, respectively. The measured resolutions ΔE_m, are

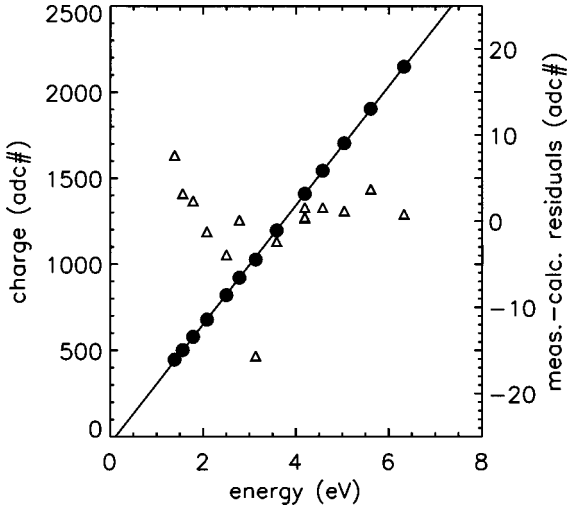

FIG. 5. Measured single photon charge output (●) as a function of photon energy for the $20\times 20\ \mu m^2$ device at $V_{bias} = 0.25$ mV and $T = 300$ mK. The solid line is a best fit of the data to a linear relation between energy and charge output. The residuals of the fit (observed-calculated) are also indicated (△).

0.55–0.70 eV for the base electrode and 0.60–0.95 eV for the top electrode. The electronic noise contribution to the energy resolution is $\Delta E_{electr} = 0.50-0.55$ eV in all measurements. Also indicated is the device-limited energy resolution ΔE_c, obtained from $(\Delta E_c)^2 = (\Delta E_m)^2 - (\Delta E_{electr})^2$. The device-limited resolution as derived from the experimental data has been compared to the theoretical resolution for a symmetrical STJ calculated from Eq. (4) with $\langle n \rangle = 4$, $\alpha = 0$ and $\sigma_{electr} = 0$, is also shown in Figs. 6(a) and 6(b). Clearly, the device-limited energy resolution of the top elec-

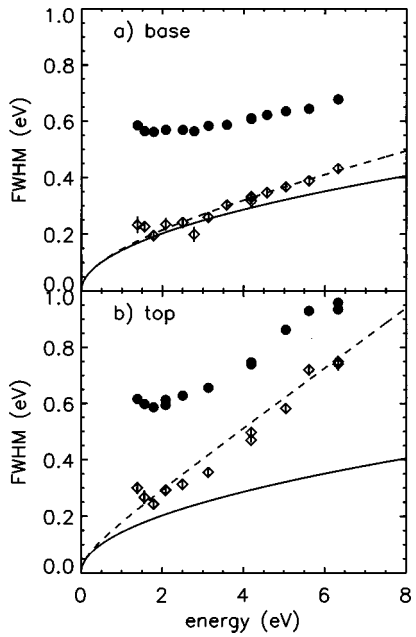

FIG. 6. The measured FWHM energy resolution (●) as a function of photon energy for (a) the base electrode and (b) the top electrode. Also indicated is the derived device-limited energy resolution (◇). The solid and dashed lines are the predicted device limited resolution without and with a contribution from spatial nonuniformities in the response, respectively.

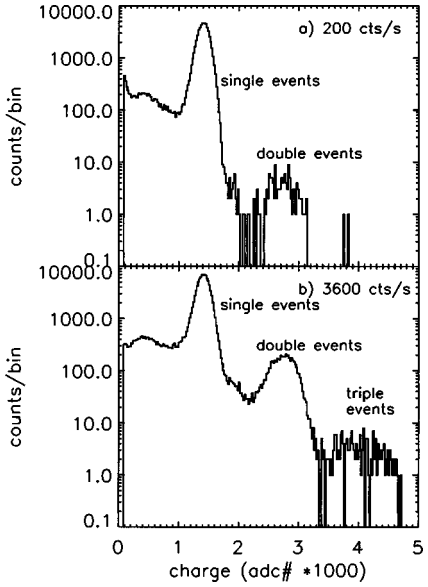

FIG. 7. Pulse height spectra at $\lambda = 300$ nm ($V_{bias} = 0.25$ mV, $T = 300$ mK, $B = 8$ mT) for the 20×20 μm^2 device at detected event rates of (a) 200 cts/s and (b) 3600 cts/s.

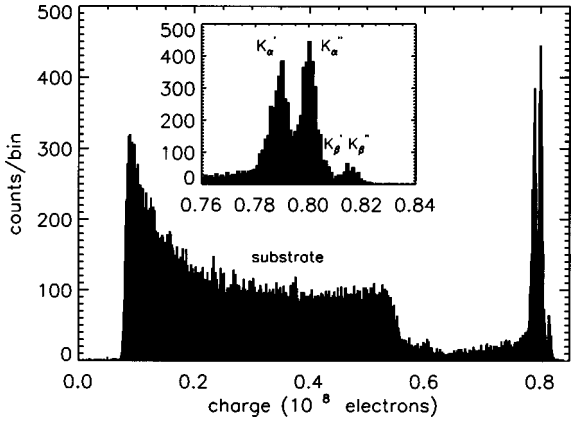

FIG. 8. Pulse height spectrum from the 20×20 μm^2 device illuminated with a ^{55}Fe source ($V_{bias} = 0.2$ mV, $T = 300$ mK, $B = 8$ mT). The insert is a zoom-in on the double set of $K\alpha$-$K\beta$ peaks at the high pulse height end of the spectrum.

trode is affected significantly by spatial nonuniformities, whereas the base electrode shows an almost theoretical behavior. This is probably related to the very different quasiparticle diffusion properties in the two films. An approximate estimate of the contribution from the spatial nonuniformity factor α to the energy resolution of the base and top electrode are $\alpha = 0.015$ eV/eV and $\alpha = 0.042$ eV/eV, respectively.

3. Count rate capability

The system's capability to deal with high event rates has been tested by varying the photon flux incident on the STJ and monitoring the quality of the single photon pulse height spectra at $\lambda = 300$ nm. Figures 7(a) and 7(b) shows the spectra at event rates of 200 and 3600 detected photons/s, respectively. Degradation of the spectra at high event rates occurs through the pile-up of events. Due to the bipolar shaping circuit, the measured pulse height for two coincident events can range from less than the amplitude of a single event to up to twice that amplitude. The double pulse height events are clearly recognized as a second peak in the high countrate spectrum of Fig. 7(b), whereas the lower pulse height events are seen as extensions of the tails of the main peak and an elevation of the low pulse height floor in the spectrum. At an event rate of 3600 cts/s, about 10% of the detected events are such pile-up events. The degradation in energy resolution (measured as FWHM of the main peak in the spectrum) at an event rate of 3600 cts/s is, however, less then 10%, and the variation in pulse height of the single photon peak is within $\pm 1\%$. It must be stressed that this pile-up effect is simply due to the relatively long event processing time of the electronics, rather than the duration of the signal pulse from the STJ, which is estimated to have a decay time of order 2 μs. No attention to minimizing the electronics process time has been given in the current experiments. For practical astronomical applications of such a device this processing time would need to be significantly reduced.

B. X-ray experiments

1. Responsivity and energy linearity

X-ray spectra have been acquired with the same 20×20 μm^2 and 50×50 μm^2 devices used for the optical experiments. Figure 8 shows a charge output spectrum from the 20×20 μm^2 device, illuminated by a ^{55}Fe source. It shows a large number of low pulse height events attributed to photons which are absorbed in the sapphire substrate, where their energy is converted into phonons, which, in their turn, can diffuse into the STJ's base electrode and break Cooper pairs into quasiparticles.[22] These are subsequently detected by their tunnel processes across the barrier. The substrate events are the majority of the events: only $\sim 4\%$ of the photons incident on the area of a STJ are actually absorbed in the superconducting films of the detector. The latter are the events of interest and they are represented by the double set of K_α and K_β peaks at the highest pulse heights. Each set corresponds to absorptions in either the top or the base niobium electrode. The difference in charge output for the two electrodes is $\sim 2\%$. The spectra show no clear indication for events related to absorptions in the aluminum films. The calculated fraction of events absorbed in the aluminum is $\sim 10\%$ of the total number of events absorbed in the STJ.[21]

The variation with bias voltage of the charge output for the K_α peak with the highest pulse height in the 50×50 μm^2 device is shown in Fig. 9(a). Maximum charge output occurs at $V_{bias} \approx 0.20$ mV for both device sizes and amounts to 2.3×10^8 electrons for the 50×50 μm^2 device and to 0.85×10^8 electrons for the 20×20 μm^2 device. This is a rather different behavior from that observed at optical wavelengths (see Fig. 4). The measured charge output is about two orders of magnitude higher than measured from similar devices with thin (5 nm) Al trapping layers.[23] The corresponding responsivities are 3.9×10^4 and 1.4×10^4

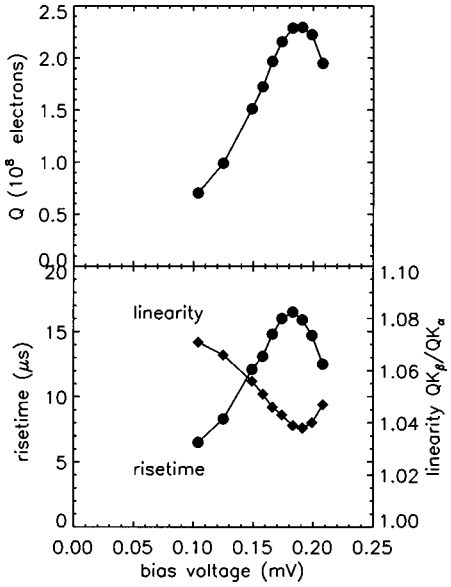

FIG. 9. The maximum Mn-$K\alpha$ charge output (a), decay time and energy nonlinearity (b) against bias voltage for the $50\times50\ \mu m^2$ device ($T=300$ mK, $B=8$ mT).

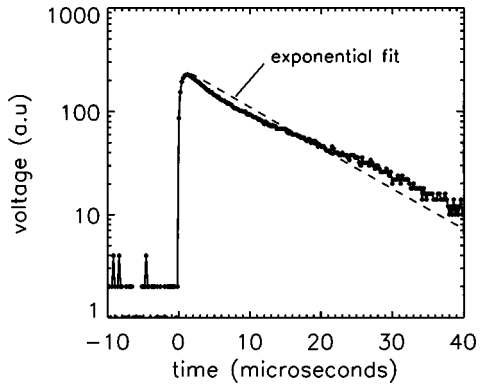

FIG. 10. A 6 keV photon x-ray pulse from the $50\times50\ \mu m^2$ device (at $V_{bias}=0.2$ mV, $T=300$ mK, $B=8$ mT), as measured at the output of a preamplifier with a RC time of 0.5 μs. The measured pulse shape is clearly different from a single exponential decay (dashed curve), indicative of a nonlinear energy response.

electrons/eV, which exceeds the responsivities at optical photon energies (see Fig. 4) by a factor of 11 and of 5, respectively.

The observed rise time of the pulses from the charge sensitive preamplifier, corresponding to the decay time of the current pulse from the STJ, also depends strongly on the bias voltage and ranges from 3–12 μs for the $20\times20\ \mu m^2$ device and from 4–20 μs for the $50\times50\ \mu m^2$ device [see Fig. 9(b)]. Again, there is a large discrepancy with the rise times in the optical experiments (see Sec. IV A 1). The strong dependence on bias voltage of the pulse decay time is rather surprising since this decay time reflects the quasiparticle life time in the detector. Mears *et al.*[7] have observed the same phenomenon in STJs of the same type, and have interpreted this as the result of a thermoelectric feedback mechanism.

In most spectra, the relative separation of K_α and K_β peaks is far less than the corresponding difference in photon energy ($E_{K\beta}/E_{K\alpha}=1.101$). The ratio of measured charge outputs $Q_{K\beta}/Q_{K\alpha}$ is 1.02 for the $20\times20\ \mu m^2$ device and 1.045 for the $50\times50\ \mu m^2$ device (at $V_{bias}=0.20$ mV). Moreover, this nonlinearity in the energy response is strongly dependent on bias voltage, as is shown in Fig. 9(b). Figure 10 shows a pulse from a 6 keV x-ray photon from the $50\times50\ \mu m^2$ device, measured at the output of a dedicated preamplifier with a RC time constant of 0.5 μs. The rising edge of the pulse is dominated by this RC time, whereas the decay of the pulse reflects the decay of the current pulse from the STJ. Clearly, the decay cannot be described by a single exponential (represented by the dashed curve). The initial fast decay is explained by the rapid self-recombination of quasiparticles when their density is high. As this density reduces due to losses, the recombination slows down until the total decay rate is dominated by the excess loss mechanisms (such as quasiparticle trapping at the edges). This severe nonlinearity in the x-ray response makes the discrepancy with the observed responsivity at optical energies even more remarkable.

2. Energy resolution

The best signal-to-noise ratio is found for the electrode with the largest pulse height for both devices and corresponds to $\Delta Q/Q=0.0068$ for the $20\times20\ \mu m^2$ device and $\Delta Q/Q=0.011$ for the $50\times50\ \mu m^2$ device. The corresponding widths of the electronic pulser at the same pulse height are 0.0022 and 0.0033, respectively. After correction for the nonlinearity of the local energy scale, the measured energy resolutions are ~150 eV and ~140 eV (FWHM) for the $20\times20\ \mu m^2$ and the $50\times50\ \mu m^2$ device, respectively. Significantly better results have been obtained with similar devices with thin (5 nm) Al layers.[23] Note that an extrapolation of the measured energy resolution for the base electrode of the $20\times20\ \mu m^2$ device in the visible/uv wavelength region would imply $\Delta E\approx210$ eV (FWHM) at $E=5895$ eV, approximately in agreement with the observed 150 eV.

V. CONCLUSIONS

High quality niobium based STJs with Al trapping layers have been demonstrated as single photon detectors in the uv-NIR wavelength region ($\lambda=200-1000$ nm, $E=1.2-6.2$ eV), and at x-ray energies ($E=5.9$ keV).

At uv-NIR photon energies, the best signal-to-noise ratio is obtained with a $20\times20\ \mu m^2$ device, operated at $T=0.30$ K. The lower energy limit for single photon detection with this device is 1.17 eV ($\lambda=1060$ nm), determined by noise of the remote room temperature electronics. The observed signal amplitudes at these wavelengths correspond to an average of 4–5 tunnel processes per quasiparticle. The response of the device is also linear with photon energy to within the measurement accuracy of a few percent. The measured energy resolution (FWHM) at low photon energy ranges from 0.55–0.70 eV for the base electrode, and from 0.60–0.95 eV for the top electrode, with an electronic noise contribution of 0.55 eV. The devices capability to deal with reasonably high photon fluxes has been demonstrated for

event rates up to 3.5 kHz. No significant degradation of the pulse height spectra is observed, other than by pile-up of events due to the relatively long event processing time of the current nonoptimized electronics.

The devices responsivity (in detected charge per eV of photon energy) at an x-ray energy of 5.9 keV was found to be 5–10 times higher than in the uv/NIR, with correspondingly longer pulse decay times. The x-ray responsivity also shows a strong nonlinearity with photon energy, which is attributed to the loss of phonons, emitted in the self-recombination process of excess quasiparticles, from the trapping volume. The processes which can account for the large discrepancy between the response in x-ray and optical wavelengths are presently being investigated in a series of experiments on devices with varying Al trapping layer thicknesses[24] as well as in experiments at intermediate photon energies ($E=10-100$ eV).

[1] N. Booth and D. J. Goldie, Supercond. Sci. Technol. **9**, 493 (1996).
[2] M. Kurakado, Nucl. Instrum. Methods **196**, 275 (1982).
[3] N. Rando, A. Peacock, A. van Dordrecht, C. L. Foden, R. Engelhardt, B. G. Taylor, J. Lumley, and C. Pereira, Nucl. Instrum. Methods Phys. Res. A **313**, 173 (1992).
[4] D. J. Goldie, P. L. Brink, C. Patel, N. E. Booth, and G. L. Salmon, Appl. Phys. Lett. **64**, 3169 (1994).
[5] C. A. Mears, S. E. Labov, and A. T. Barfknecht, Appl. Phys. Lett. **63**, 2961 (1993).
[6] P. Verhoeve, N. Rando, J. Verveer, A. van Dordrecht, A. Peacock, P. Videler, M. Bavdaz, D. J. Goldie, T. Lederer, F. Scholze, G. Ulm, and R. Venn, Phys. Rev. B **53**, 809 (1996).
[7] C. A. Mears, S. E. Labov, M. Frank, M. A. Lindeman, L. J. Hiller, H. Netel, and A. T. Barfknecht, Nucl. Instrum. Methods Phys. Res. A **370**, 53 (1996).
[8] P. Hettl, G. Angloher, M. Bruckmayer, F. von Feilitsch, J. Jochum, H. Kraus, and R. L. Mössbauer, Proceedings of the Seventh International Workshop on Low Temperature Detectors, Munich, 1997, edited by S. Cooper (unpublished), p. 20, LTD7.
[9] M. A. C. Perryman, C. L. Foden, and A. Peacock, Nucl. Instrum. Methods Phys. Res. A **325**, 319 (1993).
[10] A. Peacock, P. Verhoeve, N. Rando, A. van Dordrecht, C. Erd, M. A. C. Perryman, R. Venn, J. Howlett, D. J. Goldie, and J. Lumley, Nature (London) **381**, 135 (1996).
[11] A. Peacock, P. Verhoeve, N. Rando, M. A. C. Perryman, B. G. Taylor, and P. Jakobsen, Astron. Astrophys., Suppl. Ser. **123**, 581 (1997).
[12] T. Peacock, P. Verhoeve, N. Rando, C. Erd, M. Bavdaz, B. G. Taylor, and D. Perez, Astron. Astrophys., Suppl. Ser. **127**, 497 (1998).
[13] N. E. Booth, Appl. Phys. Lett. **50**, 293 (1987).
[14] P. Verhoeve, N. Rando, J. Verveer, A. Poelaert, A. Peacock, A. van Dordrecht, D. H. Lumb, D. J. Goldie, J. M. Lumley, and R. Venn, Proc. SPIE **2518**, 278 (1995).
[15] A. Peacock, P. Verhoeve, N. Rando, A. van Dordrecht, B. G. Taylor, C. Erd, M. A. C. Perryman, R. Venn, J. Howlett, D. J. Goldie, J. Lumley, and M. Wallis, J. Appl. Phys. **81**, 7641 (1997).
[16] N. Rando, P. Verhoeve, A. van Dordrecht, A. Peacock, M. Perryman, S. Andersson, J. Verveer, B. Collaudin, D. J. Goldie, and R. Venn, Nucl. Instrum. Methods Phys. Res. A **370**, 85 (1996).
[17] A. A. Golubov, E. P. Houwman, J. G. Gijsbertsen, J. Flokstra, H. Rogalla, J. B. le Grand, and P. A. J. de Korte, Phys. Rev. B **49**, 12 953 (1994).
[18] P. A. J. de Korte, M. L. van den Berg, M. P. Bruijn, M. Frericks, J. B. le Grand, J. G. Gijsbertsen, E. P. Houwman, and J. Flokstra, Proc. SPIE **1743**, 24 (1992).
[19] J. B. le Grand, ''X-ray response of superconductive tunnel-junctions with trapping layers'', Ph.D. thesis, University of Utrecht, The Netherlands, 1994 (unpublished).
[20] P. Verhoeve, N. Rando, A. Peacock, A. van Dordrecht, D. Lumb, D. J. Goldie, and R. Venn, Nucl. Instrum. Methods Phys. Res. A **370**, 136 (1996).
[21] J. H. Weaver, C. Krafka, D. W. Lynch, and E. E. Koch, Physik Daten, Fachinformationszentrum Nr.18-1, 1981 (unpublished).
[22] A. Poelaert, C. Erd, A. Peacock, N. Rando, P. Verhoeve, A. G. Kozorezov, and J. K. Wigmore, J. Appl. Phys. **79**, 7362 (1996).
[23] P. Verhoeve, N. Rando, P. Videler, A. Peacock, A. van Dordrecht, D. J. Goldie, J. M. Lumley, J. Howlett, M. Wallis, and R. Venn, Proc. SPIE **2283**, 172 (1994).
[24] A. Poelaert, P. Verhoeve, N. Rando, A. Peacock, D. J. Goldie, and R. Venn, Proc. SPIE **2808**, 523 (1996).